

 Open access • Journal Article • DOI:10.1038/ONC.2015.69

miR-200 promotes the mesenchymal to epithelial transition by suppressing multiple members of the Zeb2 and Snail1 transcriptional repressor complexes.

— [Source link](#) 

R. Perdigao-Henriques, R. Perdigao-Henriques, Fabio Petrocca, Gabriel Altschuler ...+7 more authors





Institutions: Universidade Nova de Lisboa, Boston Children's Hospital, Harvard University, University of Sheffield

Published on: 14 Jan 2016 - Oncogene (Nature Publishing Group)

Topics: Gene knockdown, Regulation of gene expression, Gene expression, Promoter and XBP1

Related papers:

- [The miR-200 family and miR-205 regulate epithelial to mesenchymal transition by targeting ZEB1 and SIP1.](#)
- [The miR-200 family determines the epithelial phenotype of cancer cells by targeting the E-cadherin repressors ZEB1 and ZEB2](#)
- [A reciprocal repression between ZEB1 and members of the miR-200 family promotes EMT and invasion in cancer cells](#)
- [The miR-200 family inhibits epithelial-mesenchymal transition and cancer cell migration by direct targeting of E-cadherin transcriptional repressors ZEB1 and ZEB2.](#)
- [A Double-Negative Feedback Loop between ZEB1-SIP1 and the microRNA-200 Family Regulates Epithelial-Mesenchymal Transition](#)

Share this paper:    

View more about this paper here: <https://typeset.io/papers/mir-200-promotes-the-mesenchymal-to-epithelial-transition-by-354ypepmkw>



This is a repository copy of *miR-200 promotes the mesenchymal to epithelial transition by suppressing multiple members of the Zeb2 and Snail1 transcriptional repressor complexes.*

White Rose Research Online URL for this paper:
<http://eprints.whiterose.ac.uk/93699/>

Version: Accepted Version

Article:

Perdigao-Henriques, R., Petrocca, F., Altschuler, G. et al. (5 more authors) (2015) miR-200 promotes the mesenchymal to epithelial transition by suppressing multiple members of the Zeb2 and Snail1 transcriptional repressor complexes. *Oncogene*, 35. pp. 158-172. ISSN 0950-9232

<https://doi.org/10.1038/onc.2015.69>

Reuse

Unless indicated otherwise, fulltext items are protected by copyright with all rights reserved. The copyright exception in section 29 of the Copyright, Designs and Patents Act 1988 allows the making of a single copy solely for the purpose of non-commercial research or private study within the limits of fair dealing. The publisher or other rights-holder may allow further reproduction and re-use of this version - refer to the White Rose Research Online record for this item. Where records identify the publisher as the copyright holder, users can verify any specific terms of use on the publisher's website.

Takedown

If you consider content in White Rose Research Online to be in breach of UK law, please notify us by emailing eprints@whiterose.ac.uk including the URL of the record and the reason for the withdrawal request.



eprints@whiterose.ac.uk
<https://eprints.whiterose.ac.uk/>

A genome-wide siRNA screen identifies proteasome addiction as a vulnerability of basal-like triple-negative breast cancer cells

Fabio Petrocca^{1*}, Gabriel Altschuler², Shen Mynn Tan¹, Marc L. Mendillo³, Haoheng Yan⁴, D. Joseph Jerry⁴, Andrew L. Kung⁵, Winston Hide², Tan A. Ince⁶ and Judy Lieberman^{1*}

¹Program in Cellular and Molecular Medicine, Boston Children's Hospital, and Department of Pediatrics, Harvard Medical School, Boston, MA 02115, USA

²Department of Biostatistics, Harvard School of Public Health, Boston MA 02115, USA

³The Whitehead Institute for Biomedical Research, Cambridge, MA 02142, USA

⁴Department of Veterinary & Animal Sciences, University of Massachusetts, Amherst, MA 01003, USA

⁵Department of Pediatric Oncology, Dana-Farber Cancer Institute and Children's Hospital, Boston, MA 02115, USA

⁶Department of Pathology, Braman Family Breast Cancer Institute and Interdisciplinary Stem Cell Institute, University of Miami Miller School of Medicine, Miami, FL 33136, USA

*Correspondence: fabio.petrocca@childrens.harvard.edu or

judy.lieberman@childrens.harvard.edu;

Bioinformatics correspondence: white@hsph.harvard.edu

Running Title: siRNA screen of basal-like TNBC

Summary

Basal-like triple negative breast cancers (TNBC) have poor prognosis. To identify basal-like TNBC dependencies, a genome-wide siRNA lethality screen compared two human breast epithelial cell lines transformed with the same genes - basal-like BPLER and myoepithelial HMLER. Expression of the screen's 154 BPLER dependency genes correlated with poor prognosis in breast, but not lung or colon, cancer. Proteasome genes were overrepresented hits. Basal-like TNBC lines were selectively sensitive to proteasome inhibitor drugs relative to normal epithelial, luminal and mesenchymal TNBC lines. Proteasome inhibition reduced growth of established basal-like TNBC tumors in mice and blocked tumor-initiating cell function and macrometastasis. Proteasome addiction in basal-like TNBCs was mediated by NOXA and linked to MCL-1 dependence.

Significance

There is no targeted therapy for TNBCs, which are prone to relapse and metastasize after cytotoxic drug treatment. A genome wide screen identified without bias genetic dependencies, and hence potential drug targets, of basal-like TNBCs, a common subtype. The screen led to experiments that showed that basal-like breast cancers, but not other breast cancer subtypes, are commonly addicted to the proteasome and MCL-1 and sensitive to proteasome inhibitors. Importantly, tumor-initiating cells (T-ICs) within basal-like cancers did not survive proteasome inhibition. Developing ways to target T-ICs is a priority of cancer drug development. Although bortezomib does not penetrate tumors well, our findings suggest that next generation proteasome inhibitors are worth investigating for treatment of this TNBC subtype.

Introduction

TNBC, defined by their lack of estrogen (ER), progesterone (PR) and Her2 receptors, are an especially aggressive group of tumors that typically afflict younger women and have the worst prognosis of any breast tumor subtype (Foulkes et al., 2010; Gusterson, 2009). Although most TNBC respond to cytotoxic platinum/taxane-containing regimens, they are prone to recur, metastasize and become resistant to chemotherapy (Foulkes et al., 2010; Metzger-Filho et al., 2012). TNBCs are the breast cancer subtype most enriched for poorly differentiated $CD44^+CD24^{low/-}ESA^+$ tumor-initiating cells (T-ICs), sometimes called cancer stem cells, cells thought to be responsible not just for tumor initiation, but also for metastasis and resistance to chemotherapy (Al-Hajj et al., 2003; Keller et al., 2012). Because of its poor prognosis, a better understanding of TNBC and how to treat it is needed.

TNBCs are exceedingly heterogeneous by exome and genome sequencing (Banerji et al., 2012; CancerGenomeAtlas, 2012; Curtis et al., 2012; Shah et al., 2012; Stephens et al., 2012). Some TNBCs arise in patients bearing mutations in *BRCA1* or *BRCA2*. Although mutations in *TP53* (in 63-80% of basal TNBC), *PIK3CA* (in 10% of TNBC) and *PTEN* or *RB1* (in 8% of TNBC) are common, they are also found in less aggressive breast cancers. Moreover, most mutations occur at <1% frequency in TNBCs, suggesting that these tumors might be driven by many different mechanisms. Gene expression by TNBCs is also quite varied. A recent study based on unsupervised hierarchical clustering of publicly available gene expression arrays of hundreds of primary TNBCs suggests that TNBCs can be classified based on their gene expression into at least 7 distinct subtypes (Lehmann et al., 2011). Nonetheless, the majority of TNBCs typically have an epithelial progenitor (basal-like) phenotype.

Mammalian RNAi screens have been a powerful tool to identify without bias the genetic basis for cancer-related processes including cell proliferation, migration and apoptosis, but no studies have harnessed the power of genome-wide RNAi screening to pinpoint potential vulnerabilities of TNBC (Luo et al., 2009; Zender et al., 2008). We therefore performed a genome-wide siRNA lethality screen to identify selective vulnerabilities associated with a basal-like phenotype.

Results

BPLER display a basal-like phenotype and are enriched for tumor-initiating cells

When normal human breast primary epithelial cells are grown in chemically defined WIT and MEGM media, they expand into two types of cells, epithelial progenitor cells (BPEC) and myoepithelial cells (HMEC), respectively (Figure 1A) (Ince et al., 2007). After transformation with *TERT*, *SV40 early region* and *HRAS^{V12}* in these media, they give rise to BPLER and HMLER cancer lines. Despite their shared genetic background and similar rates of proliferation, BPLER had high tumor-initiating potential, forming tumors in nude mice with as few as 50 cells, whereas 5×10^4 HMLER did not form tumors in 8 weeks (Figures 1B and 1C). Switching HMLER to WIT for 2 weeks after transformation did not affect their rate of proliferation or tumor-initiating potential (data not shown). Thus, to eliminate possible confounding effects due to differences in medium, in all subsequent experiments BPLER and HMLER were both grown in WIT. Both BPLER and HMLER lacked *ESR1*, *PGR* and *ERBB2* expression and expressed basal markers *KRT5*, *KRT14*, *KRT17* and *EGFR* (Figures S1A and S1B). Moreover they both displayed the breast T-IC phenotype ($CD44^+CD24^{low/-}ESA^+$), suggesting that these markers fall short of specifying tumor-initiating potential (Figures S1C and S1D). However, BPLER expressed intermediate levels of both E-cadherin and vimentin mRNA (Figure 1D and 1E) and stained for both basal CK14 and luminal CK18 proteins (Figure 1F), consistent with an

epithelial progenitor phenotype, while HMLER expressed ~20-fold more vimentin and negligible amounts of E-cadherin and only stained for CK14 protein, consistent with a myoepithelial phenotype.

After orthotopic transplantation in the mammary fat-pad of immunocompromised mice, BPLER initiated tumors that were histologically similar to human primary TNBC, since they were poorly differentiated epithelial lesions with focal areas of glandular differentiation, stained for both CK5 and CK14, and had high mitotic index, inflammatory infiltrates, reactive stroma and pushing borders (Figures S1E and S1F). By principal component analysis, the global transcriptional profile of six BPLER tumors from NOD/SCID mice clustered near human primary basal-like breast tumors in both the UNC337 (Prat et al., 2010) and Richardson-06 (Richardson et al., 2006) datasets (Figures 1G and S1G).

A genome-wide siRNA screen identifies 154 BPLER dependency genes

Because they were transformed with the same oncogenes, BPLER and HMLER provide an opportunity to compare selective vulnerabilities of a basal-like breast epithelial cell line enriched for T-IC with a closely related myoepithelial cell line with poor tumor-forming ability. To identify functional dependencies without bias, we performed a high throughput genome-wide siRNA lethality screen in 384-well format by transfecting BPLER and HMLER cells from the same donor in triplicate wells, each with a pool of 4 siRNAs targeting a single gene using the Dharmacon siGenome library of 17,378 gene targets. Three days later CellTiter-Glo was used to count surviving cells. The screening conditions were optimized to achieve uniform transfection and sensitivity to knockdown of *PLK1*, a gene required for mitosis, and lack of sensitivity to a non-targeting control siRNA for both cell lines (Figure 2A). Data describing the optimization of the screen are

in Figure S2. Most pools scored within 1 median absolute deviation of the plate median (Figure 2B). The ratio (R) of viable BPLER to viable HMLER cells was calculated. 1025 siRNA pools significantly decreased BPLER viability, of which 780 affected HMLER similarly. Of the remaining 245 pools, 26 were highly selectively lethal for BPLER ($R \leq 0.55$), 76 were moderately selective ($0.55 < R \leq 0.65$) and 143 were modestly selective ($0.65 < R \leq 0.75$). To validate these candidate hits, we transfected BPLER and HMLER cells separately with each of the four individual siRNAs comprising each pool. 154 of the pools reconfirmed with at least one siRNA (Figure 2C), which we defined as BPLER dependency genes. Not surprisingly, the validation rates were higher for hits with lower R values (88% of highly selective, 75% of moderately selective and 52% of modestly selective hits). The validated hits comprise a gene signature of BPLER selective dependencies. The 23 highly selective confirmed hits are shown in Figure 2D and all hits and data from the screen are provided in Figure 3 and Tables S1 and S2. 65 of the BPLER dependency genes confirmed with at least 2 individual siRNAs.

BPLER dependency genes cluster within defined functional categories

Of the 23 validated highly selective BPLER dependency genes (Figure 2D), 7 are proteasome components (hypergeometric p-value for enrichment 1.1×10^{-14}). Three other genes, the spliceosome component *PRPF8* and 2 RNA helicases (*DDX19B*, *DHX8*), are involved in mRNA biogenesis and nuclear export. The list also contains 4 Zinc finger genes (likely transcriptional activators), and a nuclear receptor coactivator gene *SNW1*, 3 genes *RAN*, *RACGAP1* and *HAUS3* that regulate the mitotic spindle and *PP2CA*, the catalytic subunit of the PP2A phosphatase.

To make sense of the 154 dependency genes, we first grouped the hits into well-defined functional categories, using a combination of the Reactome (Croft et al., 2011), KEGG

(Kanehisa et al., 2010) and Wikipathway (Pico et al., 2008) databases (Tables S3 and S4). Of the 154 genes, 121 had well described annotations that could be grouped into 13 functions with at least 3 assigned genes. The proteasome was highly over-represented with 10 proteasome subunits ($p < 3 \times 10^{-10}$) and 6 other ubiquitin proteasome system (UPS) genes. Of these, 5 genes are involved in ubiquitylation, including 2 components of the anaphase promoting complex (*ANAPC2*, *ANAPC4*), and one gene *NEDD8* that neddylates the cullins to promote mitosis. We next used GeneMANIA (Warde-Farley et al., 2010) to build a gene interaction network, incorporating physical and predicted interactions, co-localization, shared pathways and shared protein domains (Figure 3). 87 genes formed a single interacting network. Genes that participate in the major functional categories, but are not annotated to have direct protein interactions, were added to this network to produce a core functional-interaction module. The proteasome and its associated proteins constituted a core module, linking multiple dependency genes. Other broad processes that stood out were metabolism, including 2 glycolytic enzyme genes (*GAPDH*, *PFKL*), the G1/S transition and mitosis. Multiple genes involved in mRNA expression, including RNA polymerases, DNA binding proteins (likely transcriptional regulators), and mRNA splicing genes, were also hits. Most modules, and all 10 proteasome subunit genes, were in the network formed with hits reconfirming with at least 2 siRNAs (Figure S3).

Basal-like cell lines rely on BPLER dependency genes more than other breast cancers

To evaluate whether the screen captured intrinsic vulnerabilities of specific tumor subtypes, we assessed the dependence of 17 human breast cancer cell lines (Neve et al., 2006) (7 basal-A (basal-like), 6 luminal, 3 basal-B (mesenchymal) and 1 unclassified (from a squamous carcinoma)) by transfection with siRNA pools targeting 15 BPLER dependency genes implicated in the proteasome (*PSMA1*, *PSMA2*, *PSMB4*, all of which

significantly affect proteasome activity; Figure S4A), spindle checkpoint (*NDC80*, *CASC5*, *RAN*, *BUB1*, *NUF2*), metabolism (*DHRS13*, *PFKL*, *GAPDH*), molecular transport (*DDX19B*, *RFT1*), RNA splicing (*PRPF8*), and survival (*MCL1*) (Figure 4A). Cells were considered sensitive to knockdown of specific genes if viability declined to $\leq 50\%$ of control cells after 72 h. These breast cancer cell lines differed greatly in their requirements for individual BPLER dependency genes. However, basal-like cell lines shared more BPLER dependencies than non-basal-like cell lines. In fact, all 7 basal-like cell lines were dependent on at least 5 of these 15 genes, while only 2 of 6 luminal cell lines and none of the basal-B cell lines shared 5 dependencies. HCC70 and MB468 dependencies most closely resembled BPLER. Basal-like cell lines were more similar to BPLER and to each other than to non-basal-like cell lines (Figure 4B). Of note, dependency on MCL-1 was a feature of 6 of 7 basal-like cell lines, and 5 of 7 basal-like cell lines were susceptible to knockdown of at least 2 proteasome component genes, whereas non-basal-like cell lines were usually resistant. Thus although many BPLER dependencies were not shared with basal-like TNBC, most basal-like TNBCs shared dependency on the proteasome and MCL-1.

BPLER dependency gene expression correlates with poor prognosis specifically in human breast cancer

We next examined whether expression of BPLER dependency genes was associated with tumor subtype in breast cancer patients using the NKI mRNA expression profiles of 295 primary breast cancers, classified as basal-like, HER2+, luminal A, luminal B, or normal-like (van de Vijver et al., 2002). The dependency genes were significantly over-expressed in basal-like and luminal B tumors (which histologically are intermediate between basal-like and luminal A), relative to other subtypes ($p < 3 \times 10^{-5}$ and 4×10^{-6} , respectively, by Kolmogorov-Smirnov test) (Figure 4C). The same two subtypes also

significantly overexpressed the 23 validated highly selective genes ($p < 3 \times 10^{-6}$ and 4×10^{-5}). To determine whether BPLER dependency gene expression correlates with poor prognosis in breast cancer, we divided the NKI tumors into 2 groups based on expression of the 23 highly selective or 154 BPLER dependency genes. Patients with high expression of the dependency genes had significantly reduced survival and time to metastasis, which were more significant if the analysis was restricted to the highly selective hits (Figures 4D and S4B).

To validate these findings and determine whether the BPLER dependency genes are specific for breast cancer, the effect of BPLER dependency gene expression on survival and metastasis was assessed in 7 additional human tumor datasets (3 breast, 2 colon, 2 lung) comprising 1,296 human primary tumors (Figures 4E, 4F, S4B-D and Table S5) (Hou et al., 2010; Jorissen et al., 2009; Pawitan et al., 2005; Schmidt et al., 2008; Smith et al., 2010; Wang et al., 2005). In the 3 additional breast cancer cohorts, expression of the most selective and complete dependency genes again significantly correlated with poor survival and early metastasis. However, there was no significant association with survival or metastasis in colon or lung cancer. Thus, BPLER dependency gene expression correlated with poor clinical outcome specifically in breast cancer. The significant link to poor survival in breast cancer persisted even if the analysis was performed excluding all genes linked to proliferation (Figure S4E) (Venet et al., 2011). High expression of proteasome-related hits or *MCL1* was also associated with poor prognosis in breast, but not lung or colon, tumors (Figures S4F and S4G).

Many published breast cancer signatures are not significantly better outcome predictors than random signatures of identical size (Venet et al., 2011). We used the NKI dataset to compare the predictive value of the BPLER dependency genes with 1,000 randomly

generated gene signatures of the same size (Figure S4H). The 154 BPLER dependency genes and the subset of 23 highly selective hits outperformed random gene signatures ($p < 0.01$ and $p < 0.0001$, respectively). The superior predictive power of these gene sets persisted after eliminating proliferation-related genes. Thus BPLER dependency genes are up-regulated in basal-like tumors and correlate with poor prognosis selectively in breast cancer.

Proteasome inhibitors are selectively active against basal-like cell lines

Among BPLER dependencies, the proteasome stood out. Moreover, 5 of 7 basal-like cell lines were susceptible to *PSMA1* and *PSMA2* knockdown. To investigate proteasome dependence, viability of BPE (*TERT* immortalized epithelial cells, Figure 1A) and 24 breast cancer cell lines was measured 24 hr after treatment with a low concentration (12.5 nM) of the proteasome inhibitor bortezomib. Although inhibition of proteasome activity in basal-like vs. non-basal-like cell lines was comparable (Figure S5A), bortezomib was highly lethal for BPLER and basal-like cell lines compared to luminal and mesenchymal cell lines ($p < 0.001$ and $p < 0.006$, respectively; Figures 5A and S5B). Basal-like cell lines were more sensitive to bortezomib across a broad range of drug concentrations (Figure 5B). Moreover, bortezomib was only slightly cytotoxic to BPE. The in vitro LD_{50} of bortezomib for sensitive basal-like cell lines was ~5-10 nM. Carfilzomib (a second-generation proteasome inhibitor drug) also selectively killed basal-like cell lines, but was active in vitro at ~60-fold lower concentrations than bortezomib (Figures S5C and S5D and data not shown).

RAS activation and inactivation of TP53 and RB1 function are frequent in basal-like tumors. However, stable transduction of proteasome-resistant luminal MCF7 cells with active *HRAS* or dominant negative *TP53* or with an shRNA against *RB1* did not modify

their response to bortezomib, suggesting that these functional alterations were not sufficient to confer proteasome dependence (Figure S5E).

Basal-like T-ICs are sensitive to proteasome inhibition

A goal of current cancer therapeutics research is to eliminate T-ICs. To examine whether proteasome inhibitors might be active not only against the bulk of cells, but also against the T-ICs within basal-like cell lines, we examined the effect of short-term (24 hr), low-dose (12.5 nM) bortezomib exposure on *in vitro* colony and sphere formation. Basal-like cell lines that form colonies when plated at clonal density (HCC1937, HCC1143, HCC1954) lost the ability to form colonies after bortezomib treatment, whereas resistant clones emerged after paclitaxel treatment (Figure 5C and S5F). In contrast, although exposure to bortezomib or paclitaxel both reduced colony formation by luminal MCF7 and mesenchymal-like MB231 cells, resistant clones invariably emerged. Likewise, among breast cancer cell lines that form spheres under non-adherent conditions, bortezomib, but not paclitaxel, eliminated sphere-forming cells in basal-like cell lines (Figure 5D). Bortezomib also strongly inhibited sphere formation by 2 of 3 mesenchymal cell lines (MB231 and BT549, but not MB436), even though these cell lines as a whole were resistant to bortezomib, but not by 2 luminal cell lines (MCF7, BT474). Treatment with bortezomib for 24 hr also decreased viability of mouse 4T1E, a highly malignant basal-like triple negative 4T1 subclone, which is enriched for T-IC (Figure S5G-J). The ~40% of 4T1-E cells that survived bortezomib were unable to form colonies *in vitro* or initiate tumors in syngeneic mice (Figure 5E). Thus, proteasome inhibitors are active against T-ICs within basal-like cell lines.

Proteasome inhibition suppresses TNBC outgrowth and metastasis *in vivo*

To investigate whether bortezomib is effective *in vivo*, proteasome activity in BPLER tumors in nude mice was measured 18 hr after a single injection of 0.8 mg/kg bortezomib given intratumorally (i.t.), intraperitoneally (i.p.) or intravenously (i.v.) (Figure 6A). Nearly complete proteasome inhibition was achieved via i.t. injection, whereas i.p. and i.v. routes were ineffective, suggesting that bortezomib does not penetrate efficiently into tumors. However, increasing the i.v. dose to 1.6 mg/kg, the maximally tolerated dose, inhibited proteasome activity in the tumor. BPLER tumor outgrowth was evaluated by following tumor volume and measuring tumor weight at sacrifice in mice treated every 3 days i.t. (0.8 mg/kg) or weekly i.v. (0.5 or 1.6 mg/kg) after subcutaneous tumors became palpable (Figures 6B, 6C, S6A and S6B). As expected, treatment with low dose i.v. bortezomib was ineffective. Compared to control mice, tumors in bortezomib-treated mice were 85% (i.t.) and 59% (high dose iv) smaller ($p < 0.01$ and $p < 0.02$, respectively), and weighed 92% (i.t.) and 63% (high dose i.v.) less ($p < 0.001$ and $p < 0.006$, respectively). Bortezomib induced CASP3 and PARP1 cleavage in BPLER tumors, when assessed by immunohistochemistry (Figure 6D) and immunoblot (Figure 6E), suggesting that bortezomib impeded tumor outgrowth by inducing apoptosis. Likewise, weekly i.v. bortezomib (1.6 mg/kg) inhibited further growth of palpable basal-like MB468 and HCC1187 tumors (Figures 6F, 6G, S6C-E) but not luminal MCF7-*HRAS*^{V12} and AU565 tumors (Figures 6H, 6I, S6F and S6G), mirroring the *in vitro* sensitivity profile of these cell lines.

Xenografts in immunodeficient mice may not accurately reflect what happens in tumor-bearing immunocompetent hosts. We therefore also assessed the effect of bortezomib in syngeneic murine TNBC tumor models. Tumors formed in BALB/c mice orthotopically implanted with 4T1E cells were inhibited by i.v. bortezomib, even at the lower dose of 0.8 mg/kg (Figures 6J and S6H). We also assessed the effect of low and high dose i.v.

bortezomib on lung metastases that form when 4T1E cells are injected i.v. At both doses, bortezomib completely inhibited the formation of lung metastases, assessed by counting tumor nodules after intratracheal injection of India ink (Figure 6K and 6L). *Tp53*^{+/-} BALB/c mice spontaneously develop breast cancers, many of which resemble human basal-like TNBCs histologically (Yan et al., 2010). Tumor fragments from spontaneous basal-like TNBCs were implanted into the mammary fat-pad of BALB/c recipients, half of whom were treated weekly with i.v. bortezomib. Tumors in bortezomib-treated mice (1.6 mg/kg iv) were ~90% smaller and weighed ~80% less on average than in DMSO-treated mice ($p < 3 \times 10^{-6}$ and $p < 0.001$, respectively, Figures 6M, S6I and S6J). Thus, proteasome inhibition was effective in multiple models of human and mouse basal-like breast cancer in vivo.

Proteasome inhibition induces apoptosis in BPLER by promoting NOXA accumulation.

Although low-dose bortezomib inhibited proteasome activity to a similar extent (Figure S7A), BPLER cells died, but HMLER, were largely resistant (Figures S5C). Both BPLER and HMLER were equally sensitive to doxorubicin (Figure S7B). To begin to understand the molecular basis of proteasome addiction in basal-like cells, we first examined how bortezomib-treated BPLER cells died. After treatment with bortezomib for 16 hr, BPLER selectively underwent caspase-mediated apoptosis that involved mitochondrial depolarization and outer membrane permeabilization, CASP3 activation and PARP cleavage (Figures 7A, 7B, S7C, S7D). Apoptosis was inhibited by the pan-caspase inhibitor zVAD-fmk (Figure S7C) and by knocking down *BAX* and *BAK*, the bcl-2 family members that trigger the mitochondrial apoptotic pathway (Figure 7C). However, BPLER cell numbers were not completely restored by inhibiting apoptosis because bortezomib also inhibited cell proliferation (data not shown).

A targeted RNAi screen of 22 factors implicated in regulating apoptosis and the cytotoxic effect of bortezomib identified the BH3-only protein NOXA as an essential and specific mediator of the bortezomib response in BPLER (Figure 7D). Silencing *PMAIP1* (the gene encoding for NOXA) rescued BPLER cells from bortezomib comparably to zVAD-fmk. In contrast, knockdown of *BCL2L1* or *MCL1*, but not *BCL2*, augmented bortezomib-induced death. This screen suggested that other mechanisms previously linked to proteasome inhibition, such as p53 activation, NF- κ B inhibition or death receptor signaling, were not relevant in bortezomib-treated BPLER. Additional experiments also showed that bortezomib-induced cell death in BPLER was not mediated by changes in NF- κ B signaling, cellular differentiation or autophagy (Figures S7E-G). Although bortezomib caused some ER stress, treatment with any of three ER stressors for 24 hr did not induce BPLER apoptosis (Figures S7H and S7I). Bortezomib-induced death also was not blocked by co-treatment with antioxidants or ERK, MEK, p38 or JNK chemical inhibitors, suggesting that these pathways were not critical (Figure S7J).

NOXA is degraded by ubiquitylation and the proteasome (Gomez-Bougie et al., 2007). NOXA, but not other BH3-only proteins, increased dramatically in BPLER cells treated with bortezomib in the presence of zVAD-fmk (Figure S7K). NOXA protein also increased in vivo in bortezomib-treated BPLER xenografts (Figure 6E). NOXA expression was regulated both transcriptionally and post-transcriptionally, since NOXA protein increased at a low bortezomib concentration that did not alter *PMAIP1* mRNA (Figures S7L and S7M). To determine whether other pro-apoptotic BH3-only proteins contribute to bortezomib-mediated BPLER death, we examined the effect of their knockdown on BPLER viability after bortezomib treatment (Figure 7E). Only knockdown

of *PMAIP1* rescued BPLER from bortezomib. Taken together, these data suggest that NOXA mediates BPLER death from bortezomib.

NOXA accumulation and MCL-1 dependence underlie basal-like breast cancer cell line sensitivity to proteasome inhibition

We next examined whether NOXA was responsible for proteasome dependency in basal-like cells more generally. Treatment with bortezomib for 24 hr activated PARP and CASP3 cleavage in basal-like MB468, HCC1187 and HCC70 cells, but not in non-basal-like MCF7, BT474, HCC1428 cells (Figure 8A). Both basal-like and mesenchymal TNBC cell lines expressed 5-25 fold more *PMAIP1* mRNA than immortalized normal breast epithelial cells or most luminal breast cancer cell lines (Figure S8A). Treatment with bortezomib increased NOXA protein in all but one TNBC cell line, but had less of an effect on NOXA levels in immortalized breast epithelial cells and luminal cell lines (Figure 8B). Thus, the proteasome blocked accumulation of NOXA protein in most TNBC cell lines. NOXA appeared to be especially lethal in basal-like cell lines, since NOXA overexpression induced cell death in 2 basal-like cell lines (MB468 and HCC1187), but not in 2 non-basal-like cell lines (MB436 and HCC1806) (Figure S8B). Conversely, *PMAIP1* silencing inhibited bortezomib-induced death in basal-like MB468 and HCC1187 (Figure S8C).

NOXA exerts its proapoptotic effect by binding to MCL-1 and BCL2A1 (Deng et al., 2007). MCL-1, a hit in the BPLER screen, was also a dependency factor for 6 of 7 additional basal-like cell lines (Figures 4A). The amount of NOXA bound to MCL-1 increased with bortezomib treatment in basal-like MB468 and HCC1187 (Figure S8D). Moreover, *MCL1* knockdown was sufficient to induce PARP and CASP3 cleavage in basal-like MB468 and HCC1187, but not in non-basal-like MB231 and MB436 (Figure

8C). Together, these data suggest that one mechanism by which proteasome inhibition kills basal-like cell lines is by accumulation of NOXA, which in turn antagonizes MCL-1, which these cells depend on for survival. In fact, MCL-1 dependency, assessed by cell viability after MCL-1 knockdown, strongly correlated with bortezomib sensitivity in TNBC cell lines ($r=0.93$, $p<0.0005$; Figure 8D). Of note, BT20, the only bortezomib-resistant basal-like cell line, weakly expressed NOXA protein and was MCL-1-independent (Figures 4A and 8B). Steady state levels of MCL-1 were similar in proteasome sensitive and insensitive breast cancer cell lines of diverse types (Figure S8E); moreover in response to bortezomib, MCL-1 was slightly increased in both sensitive and resistant cell lines in the presence of zVAD (Figure S8F). Thus, bortezomib sensitivity of basal-like cell lines was not due to decreased MCL-1 expression.

Discussion

We used unbiased siRNA screening to uncover the functional dependencies of a basal-like TNBC cell line enriched for T-ICs as a starting point for identifying candidate drug targets of basal-like TNBCs and potentially for the subpopulation of T-ICs within them. MCL-1 and proteasome dependency were unanticipated common features of most basal-like TNBC cell lines that were only occasionally shared by other breast cancers. Treatment with a clinical proteasome inhibitor bortezomib not only inhibited basal-like tumor outgrowth, but also inhibited metastasis. Importantly, bortezomib was effective against T-ICs within basal-like TNBC cell lines – it inhibited in vitro surrogate assays of T-IC function as well as tumor initiation. This is an important finding since there are currently no effective therapies targeted at eliminating T-ICs, which are generally relatively drug-resistant and widely believed to be responsible for relapse and metastasis (Valent et al., 2012).

All cells rely on the proteasome for protein homeostasis. Therefore it might seem surprising that some cells are more dependent on this housekeeping function than others. For multiple myeloma cells, which are factories for producing and secreting immunoglobulin protein, selective proteasome dependence seems to make sense, since interfering with the ability of cells to remove unfolded proteins can lead to ER stress and apoptosis. However, why other types of cancer cells are sensitive to proteasome inhibition is not well understood. The effects of proteasome inhibition on cancer cells can lead to cell death by multiple mechanisms (Eldridge et al., 2010). Here we found that proteasome dependency in BPLER and basal-like TNBCs is linked to MCL-1 dependency and mediated by NOXA. The proteasome degrades NOXA (Ohshima-Hosoyama et al., 2011). The link to MCL-1 is not surprising since MCL-1 is an anti-apoptotic Bcl-2 family member antagonized by NOXA. A link between MCL-1, NOXA and proteasome sensitivity has already been shown in some hematopoietic malignancies (Dasmahapatra et al., 2012; Trudel et al., 2007), but not in TNBC. Moreover, MCL-1 expression is linked to poor prognosis in TNBC (Ding et al., 2007; Placzek et al., 2010). However, although NOXA is also highly upregulated by proteasome inhibition in mesenchymal TNBC lines, they are resistant to bortezomib and are not dependent on MCL-1. The reason for this difference is unclear. To take advantage of proteasome and MCL-1 dependency in developing targeted therapies for TNBCs, it will be important to understand better why basal-like TNBC are especially vulnerable to MCL-1 inhibition and why mesenchymal TNBCs are able to survive it.

The tight link we found between MCL-1 and proteasome sensitivity (Figure 8D) in TNBC could be useful for identifying tumors that will respond to proteasome inhibitor therapy. Inhibiting MCL-1, using a BH3-mimetic such as GX15-070 (Dasmahapatra et al., 2011) or lowering its expression via inhibition of cyclin dependent kinases or glucose

metabolism (Pradelli et al., 2010), might synergize with proteasome inhibition in basal-like TNBCs.

Proteasome inhibitors failed to show clinical benefit in small unstratified breast cancer trials (Awada et al., 2008; Engel et al., 2007; Schmid et al., 2008). Based on our findings, this is not surprising, since proteasome addiction is a feature of only a subset of TNBCs. TNBCs comprise only ~15% of all breast cancers and only about half of these are basal-like (Lehmann et al., 2011). Poor penetration into the tumor is a well-known limitation of bortezomib that might partly explain its lack of efficacy in solid tumors. In fact, the maximally tolerated bortezomib dose in mice was needed to achieve proteasome inhibition of xenografted tumors. At least 14 novel proteasome inhibitors are in advanced clinical development and one, carfilzomib, has been approved for multiple myeloma (Cohen et al., 2010). Proteasome inhibitors with improved pharmacokinetics and pharmacodynamics should further improve responses. It is worth evaluating these drugs in basal-like TNBCs.

Is the BPLER cell line a reasonable model for basal-like TNBCs? No individual cell line can hope to recapitulate the genetic heterogeneity of these tumors, and the oncogenes used for transformation of BPLER are not representative of TNBC mutations. Nonetheless, we chose BPLER in combination with HMLER for our screen because these two cell lines are remarkably epigenetically stable in chemically defined media in vitro with very distinct phenotypes, while harboring the same set of transforming oncogenes. BPLER have the bipotent epithelial progenitor phenotype of many basal-like TNBCs and form tumors that resemble basal-like TNBCs histologically and by gene expression. HMLER give rise to squamous tumors, a rare form of breast cancer. Thus, these two genetically well-defined, virtually isogenic cell lines offered a unique

opportunity to pinpoint selective dependencies associated with a basal-like phenotype. Although BPLER may only partially represent basal-like TNBCs, the BPLER screen identified candidate genes that might be essential for breast tumor cells locked in a progenitor-like state.

BPLER were also attractive because they are highly enriched for T-IC, which normally represent a minor subpopulation of breast cancer cell lines and are difficult to study in vitro. In fact the only other human TNBC cell line enriched for T-IC is derived from HMLER by stable knockdown of E-cadherin (HMLER-shEcad) (Gupta et al., 2009). However, HMLER-shEcad cells uniformly form mesenchymal (not basal-like) tumors in immunodeficient mice. Thus, the BPLER and HMLER-shEcad T-ICs are likely quite distinct. These results suggest that even TNBC T-ICs are heterogeneous.

Although ~18,000 genes were screened using pools of 4 siRNAs/gene, certain BPLER dependencies might have been missed, since some pools may have failed to induce sufficient gene silencing. Moreover, elimination of genes whose knockdown was lethal to both BPLER and HMLER may have discarded possible drug targets that might be effective for a broader range of breast cancers.

Our screen identified 154 BPLER dependency genes whose expression was linked to poor prognosis specifically in breast cancer, but not in colon or lung cancer. Expression of the strongest hits, only 23 genes, was just as predictive as the longer list, if not better. About 20% of these hits promote cell proliferation, but the proliferation-related genes did not explain the prognostic value of the gene list, since removing them did not seriously alter their ability to identify poor prognosis tumors. Combining the BPLER dependency gene list with lists of dependencies of other TNBCs, that need to be experimentally

identified, should provide even better prognostic gene signatures that could guide patient therapy.

The BPLER dependency gene list, which is of a manageable size, may point the way to other potential TNBC drug targets. For example, the dependency genes include glycolytic enzyme genes. In preliminary studies, we found that BPLER are selectively sensitive to glycolysis inhibition. In fact, a recent study identified glycolysis as a selective TNBC dependency (McClelland et al., 2012). A recent chemical screen in HMLER-shEcad identified the potassium ionophore salinomycin as a candidate drug (Gupta et al., 2009). Three BPLER dependency genes are potassium-sodium exchange transporters, suggesting that specific ion transport inhibition may also be effective against basal-like TNBCs. Drugs that inhibit mitosis, like paclitaxel, form the basis of current TNBC treatment. The BPLER dependency list includes multiple genes involved in mitosis. It is, however, uncertain why BPLER is selectively sensitive to inhibiting mitosis compared to other cancer cells like HMLER, which proliferate at a similar rate.

Experimental Procedures

RNAi screen. Screening was performed at the Harvard ICCB-L Screening Facility (<http://iccb.med.harvard.edu>) using the Human siGenome siRNA library (Dharmacon). Library plates with >50% of siRNA pools targeting deprecated genes (i.e. putative transcripts no longer supported by transcript evidence) were excluded. 17,378 siRNA pools, each targeting a different gene, were evaluated. Individual siRNAs in the library have not been validated. Thus the percentage of siRNA pools that effectively induce gene silencing or the extent and duration of protein knockdown, are unknown. The manufacturer estimates that most siRNA pools contain at least 1 effective siRNA. Procedures were optimized and validated for high-throughput screening under ICCB-L

guidance. Screening conditions were identical for BPLER and HMLER cells. For each cell line, each siRNA or pool of siRNAs was transfected in triplicate wells. Each microplate included 8 negative and 8 positive internal controls to monitor experimental conditions across the screen. Only microplates with a Z' factor >0.5 were analyzed (covering 98.7% of the siRNA library). Cells were dispensed with WellMate rapid plate dispensers and Teflon-coated manifolds (Matrix). siRNAs libraries were transferred into 384-well assay plates using liquid handling robots (Velocity 11 Bravo). siRNAs were reverse-transfected with Dharmafect #1 (Dharmacon) in WIT medium using a final concentration of 50 nM in 384-well white/clear microplates (Corning Cat. # 3707). Fresh medium was added after 24 hr, and cell viability was assessed by CellTiter-Glo (Promega) 3 d after transfection using an Envision high-throughput plate reader (Perkin-Elmer). A detailed description of the protocol is available upon request.

Expression analysis. Expression arrays and clinical data used in the study are listed in Table S5. Normalized expression tables were downloaded from the NCBI Gene expression Omnibus (www.ncbi.nlm.nih.gov/geo) using the R package GEOquery. The associated metadata was retrieved using GEOmetaDB. Clinical and expression data for the NKI dataset was accessed using the R package breastCancerNKI. <http://compbio.sph.harvard.edu/hidelab/pathprint> was used to map probes to unique Entrez Gene IDs, merging multiple probes by their mean expression level using systematically updated annotations obtained from AILUN. Gene expression of BPLER tumor explants was analyzed using Affymetrix arrays and Affymetrix GENECHIP software normalized using Mas5 in R.

Principal component analysis. Human breast tumor array data were obtained from two previous studies on Agilent and Affymetrix arrays (Richardson dataset (47 cases;

Richardson et al., 2006) UNC dataset (337 cases; Prat et al., 2010). Differentially expressed genes across the tumor datasets were identified using the R package Linear Models for Microarray Data (LIMMA). Array data were rank normalized using genes common across the tumor and BPLER explant arrays. Principal component analysis was based on the set of genes that differentiate the tumor datasets.

Pathway Enrichment Analysis and Network Visualization. A p-value for the over-representation of a suite of canonical pathways (KEGG, Wikipathways and Reactome) in the 154 gene signature was obtained using the hypergeometric distribution. A visualization of the interactions between the genes in the top enriched pathways was rendered using the Genemania plugin within Cytoscape (Killcoyne et al., 2009). 87 genes formed a single interacting network. Genes that participate in the major functional categories, but are not annotated to have direct protein interactions, were added to this network to produce a core functional-interaction module. Similarities in dependencies between BPLER and other breast cancer cell lines were visualized using the Prefuse Force-Directed network plugin within Cytoscape.

Code availability. The R code used to produce bioinformatic results and figures is available as Sweave files upon request.

In vivo experiments. All animal procedures were performed with Harvard Medical School and Boston Children's Hospital ACUC approval. See also supplemental experimental procedures.

Studies involving human subjects. Informed consent was not required.

Accession numbers. The mRNA microarray data from BPLER tumor explants in Figures 1G and S1G were deposited into the GEO database (GSE48444).

Acknowledgments

This work was supported by the DOD BCRP (JL, FP, SMT), the NCI (TAI; R01-CA146445) and the Breast Cancer Research Foundation (TAI). We thank Robert Weinberg for useful discussions, Caroline Shamu, Sean Johnston and Stewart Rudnicki of ICCB-Longwood for invaluable help performing the screen, Giorgia Zadra for critical advice on histopathology, Natasha Barteneva and Ken Ketman for flow cytometry assistance, and members of the Lieberman laboratory for helpful suggestions.

References:

Al-Hajj, M., Wicha, M. S., Benito-Hernandez, A., Morrison, S. J., and Clarke, M. F. (2003). Prospective identification of tumorigenic breast cancer cells. *Proc Natl Acad Sci* *100*, 3983-3988

Awada, A., Albanell, J., Canney, P. A., Dirix, L. Y., Gil, T., Cardoso, F., Gascon, P., Piccart, M. J., and Baselga, J. (2008). Bortezomib/docetaxel combination therapy in patients with anthracycline-pretreated advanced/metastatic breast cancer: a phase I/II dose-escalation study. *Brit J Cancer* *98*, 1500-1507.

Cohen, P., and Tcherpakov, M. (2010). Will the ubiquitin system furnish as many drug targets as protein kinases? *Cell* *143*, 686-693.

Croft, D., O'Kelly, G., Wu, G., Haw, R., Gillespie, M., Matthews, L., Caudy, M., Garapati, P., Gopinath, G., Jassal, B., *et al.* (2011). Reactome: a database of reactions, pathways and biological processes. *Nucl Acids Res* *39*, D691-697.

Curtis, C., Shah, S.P., Chin, S.F., Turashvili, G., Rueda, O.M., Dunning, M.J., Speed, D., Lynch, A.G., Samarajiwa, S., Yuan, Y., *et al.* (2012). The genomic and transcriptomic architecture of 2,000 breast tumours reveals novel subgroups. *Nature* *486*, 400-404.

Dasmahapatra, G., Lembersky, D., Son, M. P., Patel, H., Peterson, D., Attkisson, E., Fisher, R. I., Friedberg, J. W., Dent, P., and Grant, S. (2012). Obatoclox interacts synergistically with the irreversible proteasome inhibitor carfilzomib in GC- and ABC-DLBCL cells in vitro and in vivo. *Mol Cancer Ther* *11*, 1122-1132.

Deng, J., Carlson, N., Takeyama, K., Dal Cin, P., Shipp, M., and Letai, A. (2007). BH3 Profiling Identifies Three Distinct Classes of Apoptotic Blocks to Predict Response to ABT-737 and Conventional Chemotherapeutic Agents. *Cancer Cell* 12, 171-185.

Ding, Q., He X., Xia W., Hsu J.M., Chen C.T., Li L.Y., Lee D.F., Yang J.Y., Xie X., Liu J.C., and Hung M.C. (2007) Myeloid cell leukemia-1 inversely correlates with glycogen synthase kinase-3beta activity and associates with poor prognosis in human breast cancer. *Cancer Res* 67, 4564-71

Eldridge AG, O'Brien T. (2010) Therapeutic strategies within the ubiquitin proteasome system. *Cell Death Differ* 17, 4-13

Engel, R. H., Brown, J. A., Von Roenn, J. H., O'Regan, R. M., Bergan, R., Badve, S., Rademaker, A., and Gradishar, W. J. (2007). A phase II study of single agent bortezomib in patients with metastatic breast cancer: a single institution experience. *Cancer Invest* 25, 733-737.

Foulkes, W. D., Smith, I. E., and Reis-Filho, J. S. (2010). Triple-negative breast cancer. *New Engl J Med* 363, 1938-1948.

Gomez-Bougie, P., Wulleme-Toumi, S., Menoret, E., Trichet, V., Robillard, N., Philippe, M., Bataille, R., and Amiot, M. (2007). Noxa Up-regulation and MCL1 Cleavage Are Associated to Apoptosis Induction by Bortezomib in Multiple Myeloma. *Cancer Res* 67, 5418-5424.

Gupta, P. B., Onder, T. T., Jiang, G., Tao, K., Kuperwasser, C., Weinberg, R. A., and Lander, E. S. (2009). Identification of Selective Inhibitors of Cancer Stem Cells by High-Throughput Screening. *Cell* 138, 645-659.

Gusterson, B. (2009). Do 'basal-like' breast cancers really exist? *Nat Rev Cancer* 9, 128-134.

Hou, J., Aerts, J., den Hamer, B., van Ijcken, W., den Bakker, M., Riegman, P., van der Leest, C., van der Spek, P., Foekens, J. A., Hoogsteden, H. C., *et al.* (2010). Gene expression-based classification of non-small cell lung carcinomas and survival prediction. *PLoS One* 5, e10312.

Ince, T., Richardson, A., Bell, G., Saitoh, M., Godar, S., Karnoub, A., Iglehart, J., and Weinberg, R. (2007). Transformation of Different Human Breast Epithelial Cell Types Leads to Distinct Tumor Phenotypes. *Cancer Cell* 12, 160-170.

Jorissen, R. N., Gibbs, P., Christie, M., Prakash, S., Lipton, L., Desai, J., Kerr, D., Aaltonen, L. A., Arango, D., Kruhoffer, M., *et al.* (2009). Metastasis-Associated Gene Expression Changes Predict Poor Outcomes in Patients with Dukes Stage B and C Colorectal Cancer. *Clin Cancer Res* 15, 7642-7651.

Kanehisa, M., Goto, S., Furumichi, M., Tanabe, M., and Hirakawa, M. (2010). KEGG for representation and analysis of molecular networks involving diseases and drugs. *Nucl Acids Res* 38, D355-360.

Killcoyne, S., Carter, G. W., Smith, J., and Boyle, J. (2009). Cytoscape: a community-based framework for network modeling. *Methods Mol Biol* 563, 219-239.

Lehmann, B. D., Bauer, J. A., Chen, X., Sanders, M. E., Chakravarthy, A. B., Shyr, Y., and Pietenpol, J. A. (2011). Identification of human triple-negative breast cancer subtypes and preclinical models for selection of targeted therapies. *J Clin Invest* 121, 2750-2767.

Luo, J., Emanuele, M. J., Li, D., Creighton, C. J., Schlabach, M. R., Westbrook, T. F., Wong, K.-K., and Elledge, S. J. (2009). A Genome-wide RNAi Screen Identifies Multiple Synthetic Lethal Interactions with the Ras Oncogene. *Cell* 137, 835-848.

McClelland, M. L., Adler, A. S., Shang, Y., Hunsaker, T., Truong, T., Peterson, D., Torres, E., Li, L., Haley, B., Stephan, J. P., *et al.* (2012). An Integrated Genomic Screen Identifies LDHB as an Essential Gene for Triple-Negative Breast Cancer. *Cancer Res* 72, 5812-5823.

Mendillo, M. L., Santagata, S., Koeva, M., Bell, G. W., Hu, R., Tamimi, R. M., Fraenkel, E., Ince, T. A., Whitesell, L., and Lindquist, S. (2012). HSF1 drives a transcriptional program distinct from heat shock to support highly malignant human cancers. *Cell* 150, 549-562.

Metzger-Filho, O., Tutt, A., de Azambuja, E., Saini, K. S., Viale, G., Loi, S., Bradbury, I., Bliss, J. M., Azim, H. A., Jr., Ellis, P., *et al.* (2012). Dissecting the heterogeneity of triple-negative breast cancer. *J Clin Oncol* 30, 1879-1887.

Neve R.M. et al. (2006) A collection of breast cancer cell lines for the study of functionally distinct cancer subtypes. *Cancer Cell* 10, 515-27

Ohshima-Hosoyama, S., Davare, M. A., Hosoyama, T., Nelon, L. D., and Keller, C. (2011). Bortezomib stabilizes NOXA and triggers ROS-associated apoptosis in medulloblastoma. *J Neuro-Oncol*, 1-9.

Pawitan, Y., Bjohle, J., Amler, L., Borg, A. L., Egyhazi, S., Hall, P., Han, X., Holmberg, L., Huang, F., Klaar, S., *et al.* (2005). Gene expression profiling spares early breast cancer patients from adjuvant therapy: derived and validated in two population-based cohorts. *Breast Cancer Res* 7, R953-964.

Pico, A. R., Kelder, T., van Iersel, M. P., Hanspers, K., Conklin, B. R., and Evelo, C. (2008). WikiPathways: pathway editing for the people. *PLoS Biol* 6, e184.

Placzek W.J., Wei J., Kitada S., Zhai D., Reed J.C., and Pellecchia M. (2010) A survey of the anti-apoptotic Bcl-2 subfamily expression in cancer types provides a platform to predict the efficacy of Bcl-2 antagonists in cancer therapy. *Cell Death Dis* 1, e40.

Pradelli L.A., Bénéteau M., Chauvin C., Jacquin M. A., Marchetti S., Muñoz-Pinedo C., Auberger P., Pende M., Ricci J. E. (2010). Glycolysis inhibition sensitizes tumor cells to death receptors-induced apoptosis by AMP kinase activation leading to MCL1 block in translation. *Oncogene* 29, 1641-52.

Prat, A., Parker, J. S., Karginova, O., Fan, C., Livasy, C., Herschkowitz, J. I., He, X., and Perou, C. M. (2010). Phenotypic and molecular characterization of the claudin-low intrinsic subtype of breast cancer. *Breast Cancer Res* 12, R68.

Richardson, A. L., Wang, Z. C., De Nicolo, A., Lu, X., Brown, M., Miron, A., Liao, X., Iglehart, J. D., Livingston, D. M., and Ganesan, S. (2006). X chromosomal abnormalities in basal-like human breast cancer. *Cancer Cell* 9, 121-132.

Schmidt, M., Bohm, D., von Torne, C., Steiner, E., Puhl, A., Pilch, H., Lehr, H. A., Hengstler, J. G., Kolbl, H., and Gehrman, M. (2008). The humoral immune system has a key prognostic impact in node-negative breast cancer. *Cancer Res* 68, 5405-5413.

Shah, S. P., Roth, A., Goya, R., Oloumi, A., Ha, G., Zhao, Y., Turashvili, G., Ding, J., Tse, K., Haffari, G., *et al.* (2012). The clonal and mutational evolution spectrum of primary triple-negative breast cancers. *Nature* 486, 395-399.

Smith, J. J., Deane, N. G., Wu, F., Merchant, N. B., Zhang, B., Jiang, A., Lu, P., Johnson, J. C., Schmidt, C., Bailey, C. E., *et al.* (2010). Experimentally derived metastasis gene expression profile predicts recurrence and death in patients with colon cancer. *Gastroenterology* 138, 958-968.

Valent, P., Bonnet, D., De Maria, R., Lapidot, T., Copland, M., Melo, J. V., Chomienne, C., Ishikawa, F., Schuringa, J. J., Stassi, G., *et al.* (2012). Cancer stem cell definitions and terminology: the devil is in the details. *Nat Rev Cancer* 12, 767-775.

van de Vijver, M. J., He, Y. D., van't Veer, L. J., Dai, H., Hart, A. A., Voskuil, D. W.,

Schreiber, G. J., Peterse, J. L., Roberts, C., Marton, M. J., *et al.* (2002). A gene-expression signature as a predictor of survival in breast cancer. *New Engl J Med* 347, 1999-2009.

Venet, D., Dumont, J. E., and Detours, V. (2011). Most random gene expression signatures are significantly associated with breast cancer outcome. *PLoS Comput Biol* 7, e1002240.

Wang, Y., Klijn, J. G., Zhang, Y., Sieuwerts, A. M., Look, M. P., Yang, F., Talantov, D., Timmermans, M., Meijer-van Gelder, M. E., Yu, J., *et al.* (2005). Gene-expression profiles to predict distant metastasis of lymph-node-negative primary breast cancer. *Lancet* 365, 671-679.

Warde-Farley, D., Donaldson, S. L., Comes, O., Zuberi, K., Badrawi, R., Chao, P., Franz, M., Grouios, C., Kazi, F., Lopes, C. T., *et al.* (2010). The GeneMANIA prediction server: biological network integration for gene prioritization and predicting gene function. *Nucl Acids Res* 38, W214-220.

Yan, H., Blackburn, A. C., McLary, S. C., Tao, L., Roberts, A. L., Xavier, E. A., Dickinson, E. S., Seo, J. H., Arenas, R. B., Otis, C. N., *et al.* (2010). Pathways contributing to development of spontaneous mammary tumors in BALB/c-Trp53^{+/-} mice. *Am J Pathol* 176, 1421-1432.

Zhang, J.H., Chung, T.D. & Oldenburg, K.R. (1999) A Simple Statistical Parameter for Use in Evaluation and Validation of High Throughput Screening Assays. *J Biomol Screen* 4, 67-73.

Figure Legends

Figure 1 BPLER has a basal-like phenotype and is enriched for tumor-initiating cells compared to HMLER

(A) Schematic depicting the method used to generate BPLER and HMLER from normal breast epithelial cells. Breast organoids maintained in chemically defined media (WIT and MEGM) were sequentially transformed with retroviral vectors encoding *TERT*, *SV40 early region* and *HRAS^{V12}*. **(B)** CellTiter-Glo assay showing proliferation of BPLER, HMLER and BPE cells in WIT medium. **(C)** Tumor incidence in Nu/J mice 8 weeks after subcutaneous injection of the indicated numbers of BPLER, HMLER or MCF7 cells. **(D,E)** qRT-PCR quantification of E-cadherin **(D)** and vimentin **(E)** mRNA in BPLER and HMLER cells. **(F)** Immunofluorescence staining of cytokeratins CK14 and CK18 in BPLER and HMLER cells. Images are representative of three independent experiments. Luminal MCF7 and mesenchymal MB231 cells in **(D-F)** were used as control. **(G)** Principal component analysis of mRNA expression profiles of 6 BPLER tumors, generated in *NOD/scid* mice, and 337 human primary breast tumors classified as luminal A, luminal B, normal-like, HER2⁺, basal-like and claudin-low in the UNC337 set of primary breast cancers. The two first components are plotted with the proportion of variance explained by each component contained in the axis labels. Data in **(B)**, **(D)** and **(E)** indicate mean +/- SD. See also Figure S1.

Figure 2 Identification of BPLER selective dependencies by high throughput siRNA screening

(A) Cell viability in BPLER and HMLER transfected in high throughput screening conditions with a custom-made siRNA library containing non-targeting siRNAs (192 wells/plate) or si-*PLK1* (192 wells/plate). Each dot represents the relative CellTiter-Glo signal from individual wells at a given coordinate in three separate microplates. The Z'

factor, a measure of screening reproducibility, was calculated (Zhang et al., 1999). For both cell lines, Z' was >0.7 in each of 6 microplates transfected in two separate experiments. No significant edge effect was detected in any experiment. **(B)** Distribution of R (ratio of viability of BPLER vs HMLER) and BPLER median absolute deviation (MAD)-based Z score for all 17,378 genes in the siRNA primary screen library. The Z score measures the deviation of BPLER viability from the plate median. A Z score outside the range of -1 to $+1$ is significant. Genes were considered hits if $R < 0.75$ and the BPLER Z score was < -1.5 . Colors indicate the relative selectivity of BPLER vs HMLER lethality (green, modestly selective; blue, moderately selective; red, highly selective). **(C)** Numbers of hits in the primary screen and the confirmed hits in the secondary screen for which at least one individual siRNA from the library pool scored positive. **(D)** Confirmed highly selective BPLER dependency genes. Hits involved in specific functions are shown in different colors. See also Figure S2 and Tables S1-2.

Figure 3 BPLER dependency genes cluster within defined functional categories

Functional interaction network of BPLER dependency genes. Genes were grouped according to their participation in the indicated processes. The network was constructed using Cytoscape. The most highly selective hits are colored red. See also Figure S3 and Tables S3-4.

Figure 4 BPLER dependency genes are associated with a basal-like TNBC phenotype and are up regulated in poor prognosis breast tumors

(A) Evaluation of a subset of BPLER screening hits by knockdown in 17 human breast cancer cell lines of different subtypes. Each cell line was transfected with a control siRNA or specific siRNA pools against the indicated genes. Cell viability was assessed after 72 h. Black boxes indicate viability $\leq 50\%$ of control siRNA-transfected cells. Color

codes for breast cancer cell lines: Luminal (blue), Basal-A (red), Basal-B (green); HCC1806 and HMLER are squamous (purple). Comparable transfection efficiency (>80%) for each cell line was verified using a fluorescent siRNA and showing <50% viability after transfection with PLK1 siRNA. **(B)** Network showing the degree of similarity in dependencies between BPLER and the other breast cancer cell lines, evaluated and color-coded as in **(A)**. Cell lines with no or only 1 shared dependency are not included. Edge thickness increases with shared dependencies (max=10) and the most similar cell are closest. **(C)** Patients in the NKI database of 295 human breast primary cancers were analyzed by single sample gene set enrichment analysis (GSEA) for expression of BPLER dependency genes and the subset of highly selective genes. A Z-score for expression of the signature genes was calculated for each sample. The scores are shown as bean-plots to compare the distributions in the tumor subtypes (Basal, basal-like; Lum, luminal; NL, normal-like). Each bean consists of a green line for each sample with the overall distribution for the subtype represented as a gray density shape and a black line indicating the median Z score. **(D-F)** Breast tumors from the NKI dataset and lung and colon tumors from two independent datasets were divided into two groups based on their expression of the dependency genes (high, red; low, blue). Kaplan-Meier curves show survival in breast **(D)**, lung **(E)** and colon **(F)**, cancer patients with higher tumor expression of all dependency genes (top) or the highly selective subset (bottom). See also Figure S4 and Table S5.

Figure 5 Basal-like TNBC cells and their T-IC are selectively sensitive to proteasome inhibition

(A) Viability of 22 breast cancer cell lines 24 hr after treatment with bortezomib (12.5 nM) relative to vehicle control assessed by CellTiter-Glo. The top and the bottom of each box represent the 75th and 25th percentile of cell viability, respectively. Upper and lower

whiskers represent maximum and minimum cell viability, respectively. The black horizontal band in each box corresponds to median viability. *, $p < 0.005$; **, $p < 0.001$. Data for individual cell lines are shown in Figure S5B. **(B)** Dose-response curve of breast cancer cell lines treated with bortezomib for 24 h. Colony **(C)** and sphere formation **(D)** assays of cell lines treated with bortezomib (12.5 nM) or paclitaxel (100 nM) for 18 hr and cultured for 2 weeks in drug-free medium. Colonies were allowed to overgrow to enhance detection of slow growing colonies. **(E)** Colony formation (left) and tumor-initiation (right) of viable mouse 4T1E cells after treatment with bortezomib (12.5 nM) for 18 hr *ex vivo* (at which point ~40% of cell are viable) that were then cultured for 2 weeks in drug-free medium (colony assay) or injected in the mammary fat-pad of BALB/c mice (tumor initiation). Data in **(B,D,E)** show mean \pm SD and are representative of at least 3 independent experiments. See also Figure S5.

Figure 6 Proteasome inhibition suppresses TNBC growth in vivo

(A) Proteasome activity in protein lysates from individual subcutaneous BPLER tumors (3 mice/group) 18 hr after intratumoral (i.t), intraperitoneal (i.p) or intravenous (i.v.) treatment with bortezomib at the indicated dose, as determined by Proteasome-Glo assay, normalized by tissue weight. Proteasome activity in BPLER treated with 12.5 nM bortezomib *in vitro* is shown as control (C). Shown are the mean \pm SD of 3 replicates. Red bars indicate significant proteasome inhibition ($p < 0.05$). **(B,C)** Tumor weight in BPLER tumor-bearing mice (5 mice/group) after treatment with bortezomib or DMSO. **(D)** Immunohistochemistry of BPLER tumors treated i.t. with 0.8 mg/kg bortezomib or DMSO every 3 days. **(E)** Immunoblot of protein lysates from BPLER tumors 18 hr after a single i.v. dose of bortezomib (1.6 mg/kg) or DMSO. Each lane represents a sample from an individual mouse tumor. **(F-J)** Tumor weight in HCC1187 **(F)**, MB468 **(G)**, MCF7-HRAS^{V12} **(H)**, AU565 **(I)** and 4T1E **(J)** tumor-bearing mice after treatment with

weekly i.v. bortezomib or DMSO at the indicated dose, which was begun when tumors became palpable (50-100 mm³). HCC1187, MB468, MCF7-HRAS^{V12} and AU565 cells were injected subcutaneously. 4T1E cells were injected in the mammary fatpad. **(K,L)** Representative India-ink-stained whole lungs from BALB/c mice (4 mice/group) after i.v. injection of 2x10⁵ 4T1E cells. Beginning 2 days after 4T1E injection, mice were treated with i.v. bortezomib (0.8 mg/kg q3d or 1.6 mg/kg q7d) or DMSO. The most prominent metastatic nodules are indicated by arrows **(K)** and the mean +/- SD number of metastatic nodules determined by counting is shown in **(L)**. **(M)** Tumor weight after weekly i.v. bortezomib (1.6 mg/kg) or DMSO in mice implanted in the mammary fat pad with tumor fragments from the same spontaneously arising tumor (5 mice/group). Treatment was started 2 days after implantation. Box-and-whisker plots **(B,C,F,G,H-J,M)** show median tumor weight at time of sacrifice. *, p < 0.05. See also Figure S6.

Figure 7 Proteasome inhibition selectively induces apoptosis in BPLER by promoting NOXA accumulation

(A) Immunoblot of cells treated for 16 hr with bortezomib (12.5 nM). Each sample was assessed in duplicate independent samples. **(B)** Mitochondrial depolarization, assessed by the percentage of DiIC1(5)^{low} BPLER and HMLER cells after treatment with 12.5 nM bortezomib, was determined by flow cytometry. **(C-E)** Viability of BPLER cells transfected with the indicated siRNAs and then treated 24 hr later with 12.5 nM bortezomib or DMSO for 24 hr. zVAD-fmk was used as control. Data for each siRNA were normalized to viability of DMSO-treated cells. Data in **(B-E)** indicate mean +/- SD. See also Figure S7.

Figure 8 Bortezomib sensitivity of basal-like TNBC is linked to NOXA accumulation and MCL-1 dependency

(A-B) Immunoblot of breast cancer cell lysates treated or not with 12.5 nM bortezomib for 24 h. **(C)** Immunoblot of breast cancer cells 24 hr after transfection with an siRNA against *MCL1* or a non-targeting siRNA (control). **(D)** Scatter plot showing cell viability 72 hr after *MCL1* knockdown (x axis) and 24 hr after 12.5 nM bortezomib treatment (y axis) in TNBC cell lines and BPE cells. Color scheme in **(A-D)** as indicated in **(B)**. All data are representative of at least 3 independent experiments. *, $p < 0.05$. See also Figure S8.